12th International Conference on Fracture Mechanics of Concrete and Concrete Structures
FraMCoS-12
B.L.A. Pichler, Ch. Hellmich, P. Preinstorfer (Eds)

https://doi.org/10.21012/FC12.1326
MS02-3:1

EFFECT OF STRESS LEVEL ON HIGH CYCLE FATIGUE BEHAVIOR OF HIGH STRENGTH STRAIN HARDENING CEMENTIOUS COMPOSITE (HS-SHCC) IN COMPRESSION

DONG ZEHUA[*], ZHOU JIAJIA[†], AND ZHAO JUN[†]

[*] Zhengzhou University, School of Mechanics and Safety Engineering
Zhengzhou, China
e-mail: dongzehua0909@163.com, www.zzu.edu.cn

[†] Zhengzhou University, School of Mechanics and Safety Engineering
Zhengzhou, China
e-mail: zhouaf@zzu.edu.cn, www.zzu.edu.cn

[†] Zhengzhou University, School of Civil Engineering
Zhengzhou, China
e-mail: zhaoj@zzu.edu.cn, www.zzu.edu.cn

Key words: High strength strain hardening cementitious composite, Uniaxial compression fatigue, Fatigue creep curve, Fatigue life prediction, Three-parameter Weibull distribution

Abstract: High strength strain hardening cementitious composite (HS-SHCC) is a new type of high-performance cement-based material with excellent tensile ductility and crack control ability. Investigating the fatigue performance of HS-SHCC is of great significance for the design of engineering structures. This paper studied the influence of stress levels (0.9, 0.85, 0.8, 0.75, 0.7) on the fatigue life of HS-SHCC under uniaxial compressive fatigue loading. The failure modes were observed, and the effect of stress level on the fatigue creep curve was analyzed. The results indicate that the failure mode of the specimen under compressive fatigue was shear failure which shows little relationship with the stress level. The maximum strain of HS-SHCC display obvious three stages of rapid development, stable development and instability. The fatigue life decreases with the stress level increasing. Similar to ordinary strength SHCC, the S-N curve of HS-SHCC specimens shows a bilinear trend. Based on the obtained S-N curve and three-parameter Weibull distribution theory, a compressive fatigue life prediction model of HS-SHCC under different failure probabilities is proposed. On this basis, the maximum stress level corresponding to the fatigue strength limit (corresponding to 2 million fatigue cycles) of HS-SHCC is predicted to be 0.638.

1 INTRODUCTION

Currently, cement concrete is widely used in bridges, roads, buildings, and other engineering structures. However, there are still some inherent defects remain for concrete, for instance, low tensile strength, poor toughness, and high brittleness [1-2]. These shortcomings make concrete structures prone to cracking under varies load, thereby reducing the strength and stability of the structure. This, in return, accelerates its deterioration of the structures, exerting a negative influence on the service life of the engineering structure [3-4].

In the 1990s, Li V. C. developed a new type of engineering cementitious composite-Strain Hardening Cementitious Composites (SHCC)

principles of fracture mechanics and micromechanics [5]. The existing studies have shown that SHCCs exhibit significantly higher tensile ductility in comparison to traditional concrete (with tensile strain over 5%) and possesses strain-hardening characteristics and fine crack control abilities (crack width could be controlled below 100 μm) [6-9]. These features demonstrate its considerable potential for application in engineering structures.

When SHCCs are used in practical engineering structures, they are essentially subjected to fatigue cyclic loads from various sources. For example, in pavement and bridge deck engineering, SHCCs are required to resist the fatigue loading caused by traffic loads; in offshore wind turbine foundations and platform structures, SHCCs are exposed to cyclic loading from waves, wind, and tidal currents; and in high-rise building structures, SHCCs have to resist fatigue loading induced by wind and seismic effect [10-11]. In order to ensure the effective application of SHCCs in different projects, it is particularly important to study their fatigue behaviour deeply. Consequently, in recent years, researchers have focused on the fatigue properties of SHCC. For example, Gao et al. [12-13] investigated the effects of free water on the fatigue performance, strain evolution, damage modes, and crack propagation of SHCC under uniaxial compression, and predicted the compressive fatigue life under different water saturation conditions. Subsequent findings indicated that the fatigue life of SHCC under two-way bending exhibited superior to that under one-way bending. The bi-directional approach was employed to derive the log-normal and Weibull distribution models on the basis of the fatigue life under different failure probabilities. Based on this, the logarithmic normal distribution and Weibull distribution models were employed to estimate the fatigue life at different failure probabilities. Hu et al. [14] studied the fatigue performance of SHCC under constant lateral pressure and proposed a biaxial compression fatigue theory for SHCC. Leung C K Y et al. [15] found that SHCC-concrete composite beams exhibit higher flexural strength and longer fatigue life compared to concrete beams. Liu et al. [16] verified two damage accumulation models for SHCC based on continuous damage mechanics theory and the bending fatigue damage model through three-point bending fatigue tests on notched beam specimens. In the research by Huang et al. [17-19], the fatigue deformation behavior and fiber failure mechanisms of SHCC under tensile and compressive fatigue loads were investigated, and the mechanical response characteristics and the influence of loading frequency on the material's behavior under compressive fatigue. In the study by Huang et al. [17-20], the fatigue deformation behavior and fiber failure mechanism of SHCC under tensile and compressive fatigue loads were investigated, and the mechanical response characteristics of loading influence of loading frequency on the fatigue mechanical response characteristics and fiber action under uniaxial compression were revealed for SHCC. However, these studies primarily focus on the tensile and bending fatigue properties of SHCC, with relatively few studies addressing the compressive fatigue behavior of SHCC. Notably, researches on uniaxial compressive fatigue properties of HS-SHCC is especially scarce. As is known to all, HS-SHCC exhibits higher elastic modulus, a more compact internal structure, and enhanced wear resistance compared conventional SHCC [20-21], making it more suitable for the harsh environments. Consequently, there is a necessity to study the compressive fatigue performance of HS-SHCC.

In this paper, the fatigue failure mode and fatigue creep curve of HS-SHCC specimens under different stress levels were analysed through uniaxial compression fatigue test. Three-parameter Weibull distribution model was applied to predict the fatigue life of HS-SHCC specimens under uniaxial compression fatigue loading. The study in this paper can provide important theoretical foundation and data support for the application of HS-SHCC in practical engineering.

2 EXPERIMENTAL PROGRAM

2.1 Mix proportions

The raw materials include P·O 52.5 Ordinary Portland Cement, fine silica sand, mineral admixtures (Fly ash and Silica fume), PE fiber and superplasticizer. The PE fiber possesses a tensile strength of 3,000 MPa, a density of 0.97 g/cm3, and a volume fraction of 2%, with 18 mm in length and 24 μm in diameter. The mix proportions are shown in Table 1, and the tensile stress-strain curve is illustrated in Figure 1. It is evident from Fig. 1 that the ultimate strain of HS-SHCC under tensile load reached more than 6%, and it showed excellent multi-crack cracking characteristics. Cylinder specimens were prepared and the dimensions were 70 mm(diameter) × 140 mm(height). The specimens were demolded 24 hours after casting, followed by a 28-day curing period. Thereafter, they were placed in a room temperature environment until the test.

Table 1: Mix proportion (by mass) of HS-SHCC specimens

Unit: %

Cement	SF	FA	Sand	W	SP
60	10	30	30	18	0.696

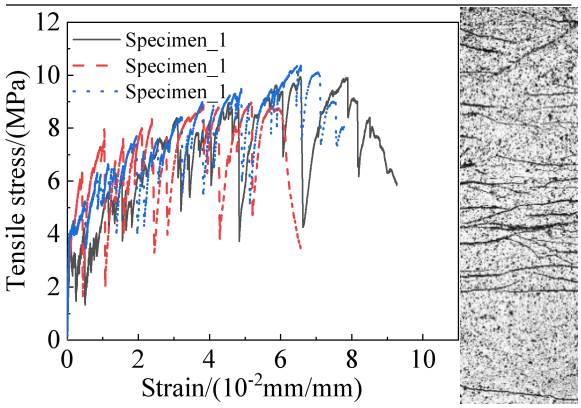

Figure 1: stress-strain curve and failure mode for HS-SHCC under uniaxial tensile loading

2.2 Testing Method

The fatigue loading test was conducted using a servo-hydraulic fatigue test system (MTS) with an ultimate bearing capacity of 500 kN. During the test, three LVDTs with a range of 25 mm were used to record the axial deformation of the specimens throughout the entire process. These LVDTs were uniformly distributed around the specimens at 120° intervals, as shown in Figure 2. The data acquisition frequency for static tests was 1 Hz, and 200 Hz for fatigue tests.

displacement control mode was applied for the static test, with a rate 0.6 mm/min. Three specimens were prepared to obtain the static uniaxial compressive strength (f_{cu}). Load control mode was used for the uniaxial compressive fatigue tests, with a frequency of 5 Hz. During the test, the maximum stress could be determined by the product of the maximum stress level S and f_{cu} ($\sigma_{max}= S\times f_{cu}$). The stress ratio ($R = F_{min}/F_{max}$) was set to 0.1. The test was terminated when one of the following conditions were met: (1) the machine displacement reached 4 mm; (2) the number of loading cycles reached 2 million. The fatigue loading spectrum is shown in Figure 3.

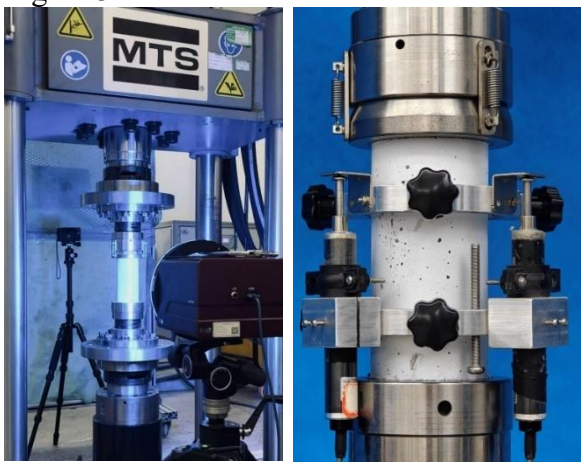

Figure 2: Compression experimental setup

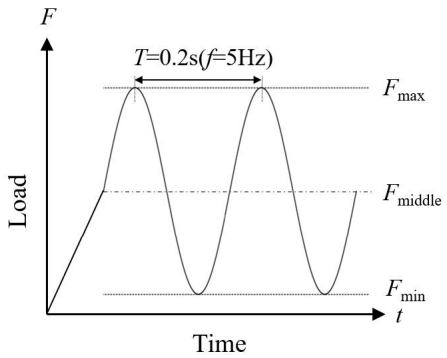

Figure 3: Compression experimental setup

3 STRESS-STRAIN CURVE OF HS-SHCC UNDER STATIC LOAD

The stress-strain curve of HS-SHCC

obtained from the static compressive test is shown in Figure 4. As is apparent from the figure, the stress-strain curve of the HS-SHCC specimen under static compressive loading could be divided into four stages: the linear elastic ascending stage (OA stage), the nonlinear ascending stage (AB stage), the descending stage (BC stage), and the residual stage (CD stage). In the linear elastic ascending stage, the stress and strain exhibited a linear relationship. At this stage, the external load was mainly borne by the matrix, with minimal contribution from the fibers. In the nonlinear ascending stage, the stress-strain curve demonstrated a nonlinear increasing trend. With an increase in the external load, cracks gradually formed and propagated. At this point, the fibers inside the HS-SHCC specimen played a bridging role, and fine cracks appeared on the surface of the specimen. Due to the high strength and high elastic modulus characteristics of HS-SHCC, its strain hardening phase was not significant. In the descending stage, the matrix and fibers were unable to withstand the external load due to the continued expansion and connectivity of microcracks, and a distinct main crack appeared on the specimen. At this point, the stress-strain curve suddenly dropped by the sudden release of energy. At the residual stage, the specimen primarily relied on the bridging effect of the fibers and the friction between the matrix on both sides of the main crack to bear the external load, so the stress-strain curve exhibited a horizontal extension trend.

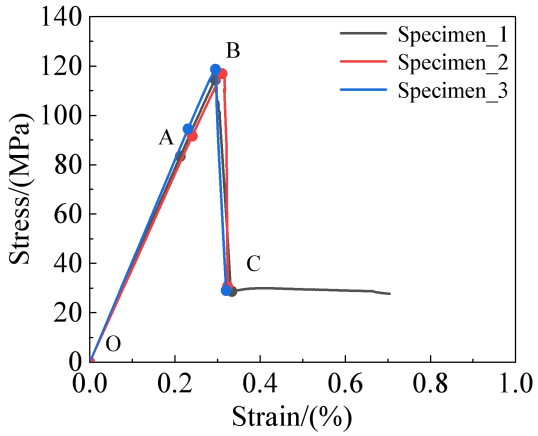

Figure 4: Compression experimental setup

The peak stress and peak strain results for each specimen are shown in Table 2. As can be seen from Table 2, the uniaxial compressive strength of HS-SHCC under static load is 116.89 MPa; the peak strain(ε_p) is 0.30443%; the elastic modulus (E) is 39.42 GPa, demonstrating high strength, high elasticity, and good deformability. The elastic modulus of HS-SHCC is almost twice that of ordinary strength SHCC (typically 10-20 GPa).

Table 2: Uniaxial compression mechanical parameters of HS-SHCC under static loading

f_{cu} (MPa)	114.35 117.49 118.83	Average of f_{cu} (MPa)	116.89
ε_p (%)	0.29546 0.31301 0.29585	Average of ε_p (%)	0.30443
E(GPa)	39.26 38.08 40.92	Average of E(GPa)	39.42

4 ANALYSIS OF THE COMPRESSION FATIGUE TEST RESULTS OF HS-SHCC

4.1 Failure Mode

Figure 5 shows the typical failure modes of HS-SHCC specimens under fatigue loading. The test results indicated that the failure mode of the HS-SHCC specimens was predominantly shear failure at all stress levels, similar to the static test results. Cracks typically developed from the top of the specimen and then extended towards the center and bottom, with distinct diagonal crack characteristics. The main crack extended along the shear plane, with the angle of propagation mainly concentrated in the 60°-90° range. This phenomenon was accompanied by the formation of numerous fine cracks. The formation of the main crack was caused by local shear stress concentration induced by fatigue loading, and it extended along the direction of maximum shear stress. The high density distribution of fine cracks was due to the bridging effect of the fibers within the HS-SHCC, which effectively controlled the propagation of the main crack. Furthermore, the incorporation of PE fibers into the HS-SHCC specimens has been demonstrated to enhance cracking control ability and toughness performance during fatigue loading, while

maintaining structural integrity up to failure.

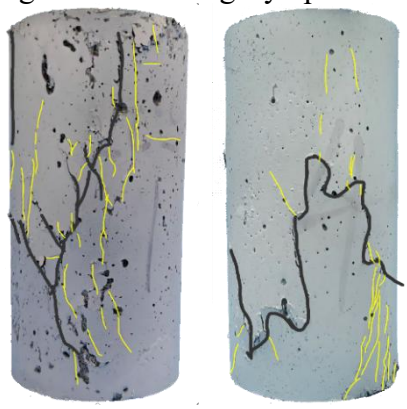

Figure 5: Failure mode of fatigue compression specimen

4.2 Fatigue creep curve

The typical fatigue creep curves of HS-SHCC specimens under different stress levels are shown in Figure 6. The vertical axis represents the maximum strain (ε_{max}) of the specimen under uniaxial compression fatigue load, while the horizontal axis denotes the relative fatigue life (the ratio of the number of cycles N to the specimen's fatigue life N_f, i.e., N/N_f). Based on the change in strain growth rate, the following three distinct stages can be observed:

(1) The rapid growth stage, which accounted for 3%–5% of the total life. The strain increase exhibited a nonlinear decreasing trend.

(2) The stable development stage, which accounted for 80%–95% of the total life. The deformation rate stabilised and increased linearly.

(3) The instability stage, which accounted for 2%–15% of the total life. The deformation rate increased significantly.

The maximum strain inflection point of normal strength SHCC typically appeared at 10-20% (the transition between the first and second stages) and 80-90% (the transition between the second and third stages) of the fatigue strain evolution curve [17]. In contrast, the fatigue strain curve of HS-SHCC exhibited an elongated S-shape, with the second stage significantly prolonged, while the first and third stages were relatively shortened. This change in stage proportions became more pronounced as the stress level decreased from 0.9 to 0.7.

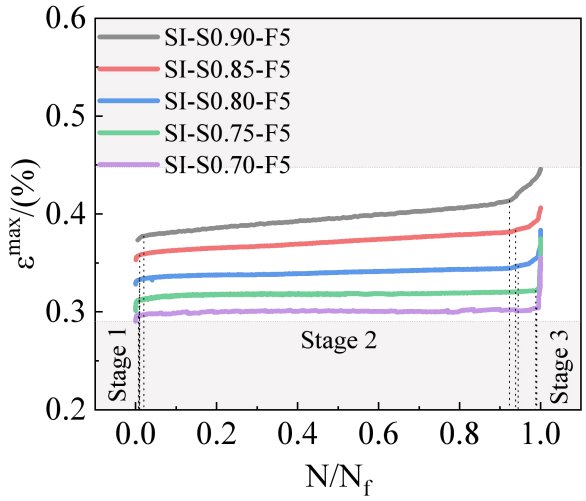

Figure 6: The relationship between the maximum strain and fatigue cycles of HS-SHCC specimens under different stress levels

4.3 Fatigue Life

Table 3 presents the fatigue life for HS-SHCC specimens under different stress levels. Specimens that did not fail after 2 million cycles were considered to have entered the "infinite life stage." As shown in Table 3, the fatigue life of the specimens gradually increased as the stress level decreased. This indicates that at lower stress levels, the material can enhance resistance to failure over fatigue loading. Furthermore, as the stress level decreases, the rate of fatigue life growth accelerates significantly. This is attributed to the slower accumulation of fatigue damage in HS-SHCC under lower loads, allowing it to sustain greater fatigue life without failure.

Table 3: Fatigue life of HS-SHCC specimens at different stress levels

Specimen No.	Stress level	Fatigue life	Average of fatigue life
SI-S0.90-F5-1	0.9	195	
SI-S0.90-F5-2	0.9	212	
SI-S0.90-F5-3	0.9	709	588
SI-S0.90-F5-4	0.9	824	
SI-S0.90-F5-5	0.9	1002	
SI-S0.85-F5-1	0.85	2043	
SI-S0.85-F5-2	0.85	4630	
SI-S0.85-F5-3	0.85	4872	5748
SI-S0.85-F5-4	0.85	8208	
SI-S0.85-F5-5	0.85	8985	
SI-S0.80-F5-1	0.8	12285	35029

SI-S0.80-F5-2	0.8	22003	
SI-S0.80-F5-3	0.8	37756	
SI-S0.80-F5-4	0.8	48787	
SI-S0.80-F5-5	0.8	54314	
SI-S0.75-F5-1	0.75	235529	
SI-S0.75-F5-2	0.75	335572	
SI-S0.75-F5-3	0.75	361566	350404
SI-S0.75-F5-4	0.75	392880	
SI-S0.75-F5-5	0.75	426474	
SI-S0.70-F5-1	0.7	676876	
SI-S0.70-F5-2	0.7	828085	
SI-S0.70-F5-3	0.7	1934226	1146396
SI-S0.70-F5-4	0.7	2000000	
SI-S0.70-F5-5	0.7	2000000	

The maximum stress level (S_{max}) and fatigue life (N_f) was established using the Wöhler equation based on the fatigue test results. This relationship can be represented by the S-N curve, as expressed by the following equation:

$$S_{\max} = A + B\log(N_f) \quad (1)$$

Where A and B are model parameters that need to be determined through fitting experimental data.

The fitted S-N curve for HS-SHCC specimens is:

$$S_{\max} = \begin{cases} -0.06244\log(N_f) + 1.08575 & (0.85 \le S_{\max} < 0.9) \\ -0.03908\log(N_f) + 1.00171 & (0.7 < S_{\max} \le 0.85) \end{cases} \quad (2)$$

This study conducted a comparative analysis of the S-N curves of HS-SHCC, ordinary strength SHCC [17], and high-strength concrete [22], as illustrated in Figure 8. The results indicate that the S-N curves of HS-SHCC and ordinary SHCC specimens under uniaxial compression fatigue loading exhibit bilinear characteristics, whereas the S-N curve of ordinary concrete specimens shows a typical linear decline. This discrepancy may be attributed to the fiber bridging effect. As demonstrated in Figure 7, the slope of the S-N curve for HS-SHCC is slightly greater than that of ordinary SHCC, indicating that the higher the strength grade of SHCC, the shorter its fatigue life, particularly at lower stress levels. This is because the toughness and ductility of the HS-SHCC matrix are lower than those of ordinary SHCC, making it more prone to brittle damage under fatigue loading. In addition, the weakening of the fiber bridging effect and the accelerated damage accumulation contribute to the significantly diminished fatigue life of HS-SHCC in comparison to that of ordinary SHCC.

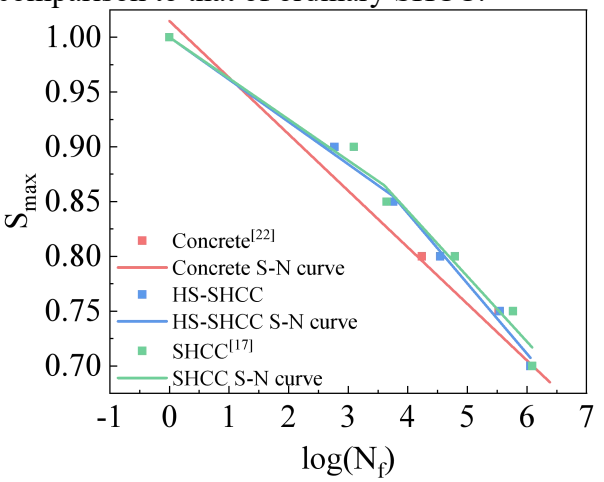

Figure 7: Max stress level and logarithmic fatigue life curve

However, due to the significant variability in the fatigue life of SHCC specimens under the same test parameters, direct prediction of fatigue life from the S-N curve is unreliable. Consequently, to enhance the precision of predictions, it is imperative to adopt more conservative and secure prediction methods.

5 FATIGUE LIFE PREDICTION AND FATIGUE STRENGTH OF HS-SHCC

5.1 Probability distribution function of fatigue life

In this paper, the three-parameter Weibull distribution model was selected for fatigue life analysis. The simplified probability density function is employed as follows:

$$f(N_f) = \frac{\beta}{\eta}\left(\frac{N_f - \gamma}{\eta}\right)^{\beta-1} \exp\left[-\left(\frac{N_f - \gamma}{\eta}\right)^{\beta}\right] \quad (3)$$

Where β, γ and η represent the shape parameter, location parameter, and scale parameter, respectively, while N_f denotes the fatigue life.

The cumulative distribution function for this model is:

$$F(N_f) = P(N < N_f) = 1 - \exp\left[-\left(\frac{N_f - \gamma}{\eta}\right)^{\beta}\right] \quad (4)$$

Where P is the failure probability.

Thus, the expression of the reliability function is :

$$P(N_f) = 1 - F(N_f) = \exp\left[-\left(\frac{N_f - \gamma}{\eta}\right)^{\beta}\right] \quad (5)$$

5.2 Distribution parameters

In this paper, correlation coefficient optimization was applied to determine the parameters of the three-parameter Weibull distribution, transforming equation (6) to simplify the fatigue life into a linear form for easier parameter estimation.

$$\ln\left[-\ln\left(1 - F(N_f)\right)\right] = \beta\left[\ln(N_f - \gamma) - \ln\eta\right] \quad (6)$$

The relationship between $ln[-ln(1-F(N_f))]$ and $ln(N_f - \gamma)$ is linear. Let $Y=ln[-ln(1-F(N_f))]$ 、 $X=ln(N_f - \gamma)$. To achieve the best linear fit for scatter points (X, Y) on the X-Y plane, this study maximized the linear correlation coefficient R(γ) to determine the parameter γ. When |R(γ)|reaches its maximum, the linear relationship is strongest, ensuring the best fit. The parameter γ was calculated using equations (7) and (8).

$$R(\gamma) = \frac{\sum_{i=1}^{n}\left[\ln\ln\frac{1}{1-F(N_{fi})}\right]\left[\ln(N_{fi}-\gamma)\right] - \frac{1}{n}\sum_{i=1}^{n}\left[\ln\ln\frac{1}{1-F(N_{fi})}\right]\sum_{i=1}^{n}\left[\ln(N_{fi}-\gamma)\right]}{\sqrt{\left\{\sum_{i=1}^{n}\left[\ln(N_{fi}-\gamma)\right]^2 - \frac{1}{n}\sum_{i=1}^{n}\left[\ln(N_{fi}-\gamma)\right]^2\right\}\cdot\left\{\sum_{i=1}^{n}\left[\ln\ln\frac{1}{1-F(N_{fi})}\right]^2 - \frac{1}{n}\sum_{i=1}^{n}\left[\ln\ln\frac{1}{1-F(N_{fi})}\right]^2\right\}}} \quad (7)$$

$$\frac{d\left|R(\gamma)\right|}{d\gamma} = 0 \quad (8)$$

With the location parameter γ determined, regression analysis provided the shape β and scale η parameters. Table 4 lists the Weibull parameters for five stress levels, and Figure 9 shows the fit between $Y=ln[-ln(1-F(Nf))]$ and $X=ln(Nf - \gamma)$, confirming good agreement with the experimental data.

Table 4: Distribution parameters of the three-parameter Weibull model for the fatigue life of HS-SHCC specimens

S	γ	β	η
0.9	191.1277	0.3458	438.8478
0.85	1021.494	1.03675	5944.6872
0.8	6142.504	1.0128	36057.1832
0.75	117764.5013	2.2402	271633.4243
0.7	484769.8196	0.82889	1284302.662

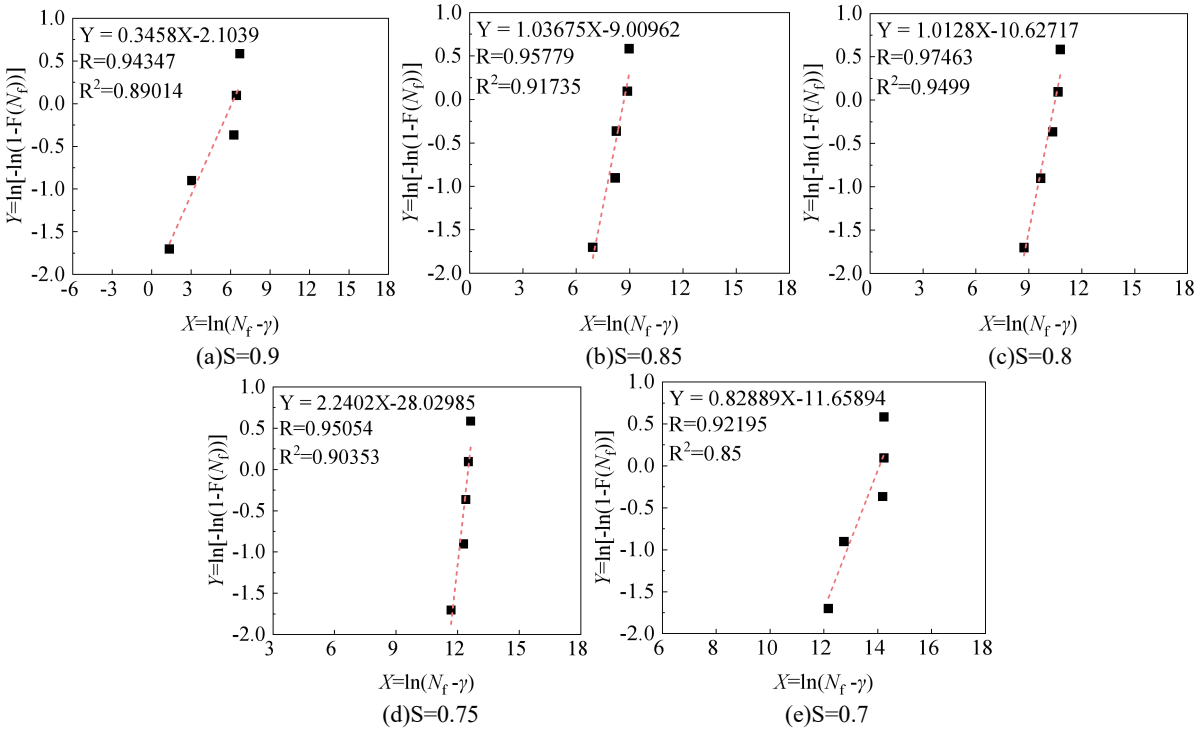

(a)S=0.9 (b)S=0.85 (c)S=0.8

(d)S=0.75 (e)S=0.7

Figure 8: Three-parameter Weibull distribution test fitting results

5.3 P-S-N equation

In engineering, the fatigue life of HS-SHCC is discrete, and the traditional S-N curve is inadequate to fully reflect the failure risk. The incorporation of failure probability in the formulation of P-S-N equation facilitates a more precise evaluation for the fatigue performance of HS-SHCC. The failure probability P could be calculated by Equation (4).

$$P = 1 - \exp[-\left(\frac{N_{\mathrm{f}} - \gamma}{\eta}\right)^{\beta}] \quad (4)$$

Then N_f is :

$$N_f = \eta[\ln(\frac{1}{1-P})]^{\frac{1}{\beta}} + \gamma \quad (9)$$

Using the parameters of the Weibull distribution, the equivalent fatigue life of HS-SHCC at different failure probabilities can be calculated as shown in Table 5. By performing a logarithmic linear fit on the data in Table 5, a series of S-N curve equations for different failure probabilities are obtained as shown in Table 6.

Table 5: Equivalent fatigue life of HS-SHCC under different failure probabilities

P	0.90	0.85	0.80	0.75	0.70
0.05	191.2	1360.3	8062.7	189903.3	520451.3
0.1	191.8	1699.8	10051.1	217240.3	569804.1
0.2	196.9	2420.5	14342.4	256823.3	695040.3
0.5	343.2	5195.9	31251.5	348401.8	1310112.3
0.95	10669.3	18150.9	112672.7	561055.4	5310202.6

Table 6: Fatigue life equations of HS-SHCC under different failure probabilities

P	Fatigue life equation	R^2	Fatigue strength-stress level
0.05	$\lg S = -0.02377 \lg N_{\mathrm{f}}$ $(1 < N_{\mathrm{f}} < 10^{4.00})$	0.9819	0.638
	$\lg S = -0.06843 \lg N_{\mathrm{f}} + 0.2362$ $(N_{\mathrm{f}} > 10^{4.00})$	0.9998	
0.1	$\lg S = -0.02125 \lg N_{\mathrm{f}}$ $(1 < N_{\mathrm{f}} < 10^{4.00})$	0.9856	0.687
	$\lg S = -0.0294 \lg N_{\mathrm{f}} + 0.02197$ $(N_{\mathrm{f}} > 10^{4.00})$	0.9398	
0.2	$\lg S = -0.02057 \lg N_{\mathrm{f}}$ $(1 < N_{\mathrm{f}} < 10^{4.00})$	0.9988	0.688
	$\lg S = -0.03172 \lg N_{\mathrm{f}} + 0.03731$ $(N_{\mathrm{f}} > 10^{4.00})$	0.9564	
0.5	$\lg S = -0.01869 \lg N_{\mathrm{f}}$ $(1 < N_{\mathrm{f}} < 10^{4.00})$	0.9985	0.696
	$\lg S = -0.03465 \lg N_{\mathrm{f}} + 0.061$ $(N_{\mathrm{f}} > 10^{4.00})$	0.9659	
0.95	$\lg S = -0.01411 \lg N_{\mathrm{f}}$ $(1 < N_{\mathrm{f}} < 10^{4.25})$	0.9192	0.720
	$\lg S = -0.0346 \lg N_{\mathrm{f}} + 0.07659$ $(N_{\mathrm{f}} > 10^{4.25})$	0.9975	

Figure 9 shows the predicted compression fatigue life of HS-SHCC at different failure probabilities, ranging from 0.05 to 0.95). All data points fall within the 0.05-0.95 range. Data points are positioned to the right of the 0.05 failure probability model, indicating a higher fatigue life than predicted. This indicated that the proposed model is suitable for engineering design with adequate safety margin. However, some data points are positioned to the left of the 0.5 and 0.95 models, showing unreliability of these models in predicting the fatigue life for HS-SHCC. Thus, the 0.05 failure probability model is recommended. The corresponding maximum stress level for HS-SHCC's fatigue limit at this probability is 0.638, providing a crucial reference for the designation of the HS-SHCC members under fatigue loading.

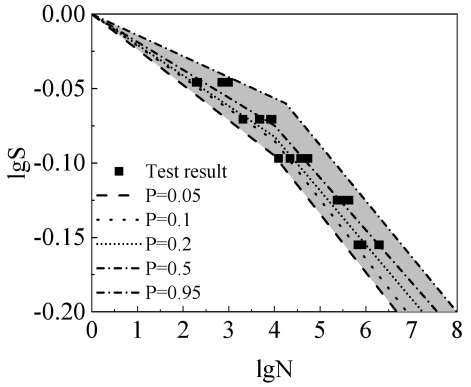

Figure 9: Prediction results of S-N model with different failure probabilities

12 CONCLUSIONS

In this paper, uniaxial compressive fatigue tests were conducted to analyse the fatigue creep curves and fatigue life for HS-SHCC under constant amplitude loading conditions. A fatigue life prediction model for HS-SHCC specimens at different failure probabilities was developed using the three-parameter Weibull distribution model. The main findings are summarized as follows:

(1) Under uniaxial compressive fatigue loading, the specimens exhibited a failure mode characterised by shear failure, showing a trend independent on the stress level. Due to the fiber bridging effect, numerous fine cracks accompanied the main crack around the failure area.

(2) The ε_{max} of HS-SHCC specimens exhibits a three-stage development trend: rapid development stage, stable development stage, and instability stage. The stress level has a significant influence on all three stages. The fatigue stress level not only affects the variation of ε_{max} in HS-SHCC specimens but also determines the lifetime distribution of the three stages.

(3) The S-N curves of HS-SHCC specimens exhibit distinct bilinear characteristics.

(4) The compression fatigue life prediction equation of HS-SHCC material under different stress levels was constructed by using the three-parameter Weibull distribution model. This model enabled the prediction of the maximum stress level corresponding to the fatigue strength limit of HS-SHCC to be 0.638 when the failure probability is 0.05.

REFERENCES

[1] Li V C. From micromechanics to structural engineering the design of cementitious composites for civil engineering applications[J]. *Doboku Gakkai Ronbunshu,* 1993, 1993(471): 1-12.

[2] Chen Zhaoyuan, Xu Youlin, Qian Jiaru. Safety and durability of structural works in civil engineering [J]. *Architecture Technology*, 2002, 33(4): 248-253.

[3] Czarnecki L, Kowalski L. Durability of concrete structures under aggressive environmental conditions [J]. *Construction and Building Materials*, 2007, 21(3): 591-598.

[4] López M L, Hernández M. Fatigue behavior of concrete under repeated loading [J]. *Materials and Structures*, 2012, 45(8): 1229-1237.

[5] Li V C, Leung C K Y. Steady-state and multiple cracking of short random fiber composites[J]. *Journal of engineering mechanics*, 1992,118(11): 2246-2264.

[6] Li V C. Process and application of engineered cementitious composites [J]. *Journal of the Chinese Ceramic Society*, 2007, 35(4): 531-536.

[7] Xu Shilang, Li Hedong. Research progress and engineering application of ultra-high toughness cementitious composites [J]. Journal of Civil Engineering, 2008, (06): 45-60.

[8] Yu J, Yao J, Lin X, et al. Tensile performance of sustainable Strain-hardening cementitious composites with hybrid PVA and recycled PET fibers[J]. *Cem Concr Res* 2018, 107:110–23.

[9] Zhou J, Pan J, Leung CKY. Mechanical behavior of fiber-reinforced engineered cementitious composites in uniaxial compression[J]. *J Mater Civ Eng* 2015, 27(1):04014111.

[10] Smith J, Brown A. Fatigue behavior of cement-treated soils under traffic loading[J]. *Journal of Transportation Engineering* 2005, 131(2): 105-113.

[11] Johnson M, Liu R. Fatigue behavior of cementitious materials in marine and

seismic environments[J]. *Journal of Materials Science and Engineering* 2008, 27(4): 251-258.

[12] Gao S, Xu Q, Wang Z, et al. Effect of water saturation on uniaxial constant amplitude tensile fatigue performance of ECC and its statistical analysis of fatigue life[J]. *International Journal of Fatigue,* 2025, 190: 108666.

[13] Gao S, Zhang J, Zhang H, et al. Study on biaxial bending fatigue performance of Engineered Cementitious Composites (ECC)[J]. *Journal of Building Engineering*, 2024, 84: 108478.

[14] Hu G, Gao S, Zhu Y. Study on ECC compression fatigue under different constant lateral compression levels[J]. *International Journal of Fatigue*, 2022, 156: 106630.

[15] Leung C K Y, Cheung Y N, Zhang J. Fatigue enhancement of concrete beam with ECC layer[J]. *Cement and Concrete Research,* 2007, 37(5): 743-750.

[16] Liu W, Xu S, Feng P. Fatigue damage propagation models for ductile fracture of ultrahigh toughness cementitious composites[J]. *International Journal of Damage Mechanics*, 2017, 26(6): 919-932.

[17] Huang B T, Li Q H, Xu S L, et al. Fatigue deformation behavior and fiber failure mechanism of ultra-high toughness cementitious composites in compression[J]. *Materials & Design*, 2018, 157: 457-468.

[18] Huang B T, Li Q H, Xu S L, et al. Tensile fatigue behavior of fiber-reinforced cementitious material with high ductility: Experimental study and novel PSN model[J]. *Construction and Building Materials,* 2018, 178: 349-359.

[19] Huang B T, Li Q H, Xu S L, et al. Frequency effect on the compressive fatigue behavior of ultrahigh toughness cementitious composites: experimental study and probabilistic analysis[J]. *Journal of Structural Engineering*, 2017, 143(8): 04017073.

[20] RANADE R, LI V C, HEARD W F, et al. Impact resistance of high strength-high ductility concrete[J]. *Cement and Concrete Research*, 2017, 98: 24-35.

[21] Sahmaran M, Li V C. Durability of mechanically loaded engineered cementitious composites under highly alkaline environments[J]. *Cem Concr Compos* 2008, 30(2):72–81.

[22] Baktheer A, Chudoba R. Experimental and theoretical evidence for the load sequence effect in the compressive fatigue behavior of concrete[J]. *Materials and Structures*, 2021, 54(2): 82.